

Electron correlations in the kagome flat band metal CsCr₃Sb₅

Fang Xie,^{1,2} Yuan Fang,¹ Ying Li,³ Yuefei Huang,⁴ Lei Chen,¹ Chandan Setty,¹ Shouvik Sur,¹ Boris Yakobson,⁴ Roser Valentí,⁵ and Qimiao Si¹

¹*Department of Physics & Astronomy, Rice Center for Quantum Materials, Rice University, Houston, Texas 77005, USA*

²*Rice Academy of Fellows, Rice University, Houston, Texas 77005, USA*

³*MOE Key Laboratory for Nonequilibrium Synthesis and Modulation of Condensed Matter, School of Physics, Xi'an Jiaotong University, Xi'an 710049, China*

⁴*Department of Materials Science and NanoEngineering, Rice University, Houston, Texas 77005, USA*

⁵*Institut für Theoretische Physik, Goethe-Universität Frankfurt, Max-von-Laue-Strasse 1, 60438 Frankfurt am Main, Germany*

(Dated: March 7, 2024)

Kagome metals offer a unique platform for investigating robust electron-correlation effects because of their lattice geometry, flat bands and multi-orbital nature. In the cases with active flat bands, recent theoretical studies have pointed to a rich phase diagram that contains not only electronic orders but also quantum criticality. CsCr₃Sb₅ has emerged as a strong candidate for exploring such new physics. Here, using effective tight-binding models obtained from *ab initio* calculations, we study the effects of electronic correlations and symmetries on the electronic structure of CsCr₃Sb₅. The effective tight-binding model and Fermi surface comprise multiple Cr-*d* orbitals and Sb-*p* orbitals. The introduction of Hubbard-Kanamori interactions leads to orbital-selective band renormalization dominated by the *d_{xz}* band, concurrently producing emergent flat bands very close to the Fermi level. Our analysis sets the stage for further investigations into the electronic properties of CsCr₃Sb₅, including electronic orders, quantum criticality and unconventional superconductivity, which promise to shed much new light into the electronic materials with frustrated lattices and bring about new connections with the correlation physics of a variety of strongly correlated systems.

Introduction. Materials with flat bands from frustrated lattices provide a distinctive venue to explore the intersection of lattice geometry, strong correlation effects and multi-orbital physics [1–10]. Experiments in such materials have found evidence for non-Fermi liquid behavior [11–13]. Theoretically, the coupling between the flat and wide bands has been shown to yield quantum phase transitions from electronic orders to paramagnetic ground states, with the quantum critical regime displaying strange metal behavior [14, 15]. The recent discovery of CsCr₃Sb₅ [16], a Cr-based kagome material, has opened an exciting avenue for exploring this rich physics while adding a new member to the kagome material family [17]. With its unique phenomenology and multi-orbital nature, this compound offers a rare opportunity to examine the robust effects of electron correlation in a flat-band platform.

CsCr₃Sb₅ is isostructural to the vanadium-based kagome material family AV₃Sb₅ (*A* = Cs, K, Rb) [18–21]. It is a bad metal at ambient pressure supporting the existence of strong correlation effects. Anomalies in transport and thermodynamic properties suggest multiple ordering transitions as a function of temperature and pressure [16]. While the nature of the order is presently unclear, its ordering vector differs from the vanadium family [4, 22–27], with a single wave-vector modulation, no doubling or quadrupling along the *c* axis, and a hexagonal to monoclinic distorted phase [16].

High temperature susceptibility data shows a Curie-Weiss behavior indicating the existence of local moments with substantial magnetic frustration. High pressure suppresses the density-wave ordering, leading to dome-like unconventional superconductivity separated by a putative quantum critical point; in contrast, the AV₃Sb₅ family exhibits ambient pressure superconductivity, which persists under pressure [21].

In addition, resistivity data indicate strong deviations from Fermi-liquid behavior further supporting the role of strong correlations and quantum criticality [16].

Here, we study the correlation physics of CsCr₃Sb₅, using effective tight-binding models to uncover the symmetries, Fermi surface, and interaction-induced band renormalization effects that shape these physical properties. Importantly, we clarify the role of strong correlation effects on the electronic structure by investigating the suppression of the orbital-dependent quasiparticle weights using the slave-spin approach. We begin by identifying the site-symmetry groups and representations of Wyckoff positions of the space group *P6/mmm*, which correspond to the lattice sites of Cr and Sb atoms in CsCr₃Sb₅. We then analyze the band structure obtained from *ab initio* calculations, which illustrates that all five *d* orbitals from the chromium atoms and all three *p* orbitals from the antimony atoms are responsible for the physics around the Fermi level. Therefore, an effective 31-band tight-binding model, which contains all of these orbitals can be constructed. By using this effective tight-binding model, we find that the introduction of Hubbard-Kanamori-type interactions [28, 29] induces strong renormalization effects in the Cr-*d* orbitals, especially the *d_{xz}* orbital, indicating orbital-selective correlations. Additionally, our analysis of the density of states and coherent band structure reveals that strong correlations cause the large spectral weight above the Fermi energy to shift towards the Fermi level. Our investigation sets the stage for further research into the nature of the ordering, superconductivity, non-Fermi liquid behavior, and other intriguing properties of this promising new material.

This manuscript is organized as follows. We first discuss the representations of the site symmetry groups of each active

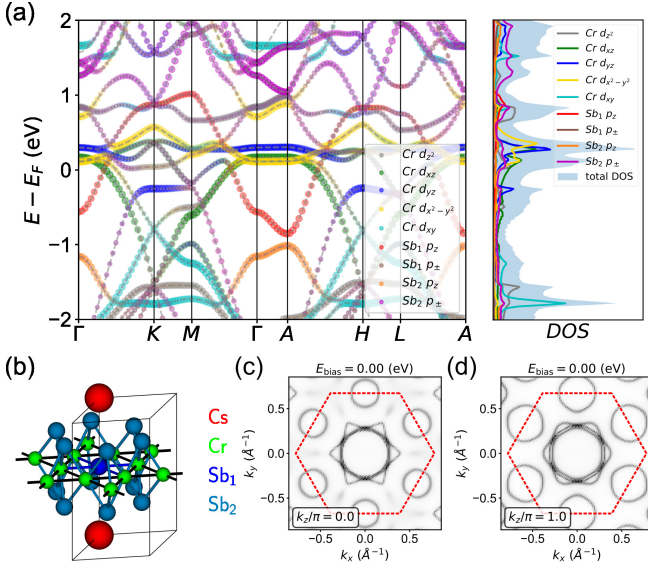


FIG. 1. (a) Band structure and local density of states of CsCr_3Sb_5 compound obtained from density functional theory using VASP and GGA. The color codes represent the orbital content of the corresponding Bloch states. (b) The lattice structure of CsCr_3Sb_5 . Black box stands for the unit cell. (c-d) Momentum-resolved spectral function at $k_z = 0$ and $k_z = \pi$ planes at the Fermi energy obtained from the DFT band structure. The red dashed line stands for the first Brillouin zone. Electron pockets near the M points, electron & hole pockets around Γ point can be seen in this spectral function. Spin-orbital coupling (SOC) is not considered.

E	C_{2x}	C_{2y}	C_{2z}	irrep	orbital
+1	+1	+1	+1	A_g	$d_{z^2}, d_{x^2-y^2}$
+1	-1	-1	+1	B_{1g}	d_{xy}
+1	-1	+1	-1	B_{2g}	d_{xz}
+1	+1	-1	-1	B_{3g}	d_{yz}

TABLE I. Irreducible representations of d-orbitals in the point group $mmm (D_{2h})$ of the $3f$ Wyckoff position of space group 191. Since all d-orbitals have inversion eigenvalue +1, the three two-fold rotations distinguish their irreps.

orbital in CsCr_3Sb_5 , and the basic properties of the effective 31-band tight-binding model are discussed. Based on the effective 31-band tight-binding model, we study the correlation effects of the Cr-d orbitals.

Symmetry and effective model. The CsCr_3Sb_5 compound has nine atoms per unit cell. As shown in Fig. 1(b), there are three chromium atoms forming a Kagome lattice. Among the five antimony atoms, one of them is at the center of the hexagon plaquette of the chromium Kagome lattice within the chromium plane denoted as Sb_1 , while the other four are at out-of-plane positions denoted as Sb_2 , forming two sets of hexagonal lattices. The antimony atoms above and below the chromium plane form two sets of hexagonal lattices. Besides, the caesium atom is positioned atop of the in-plane antimony atom in a separate plane.

The active orbitals near the Fermi level are the Cr-3d or-

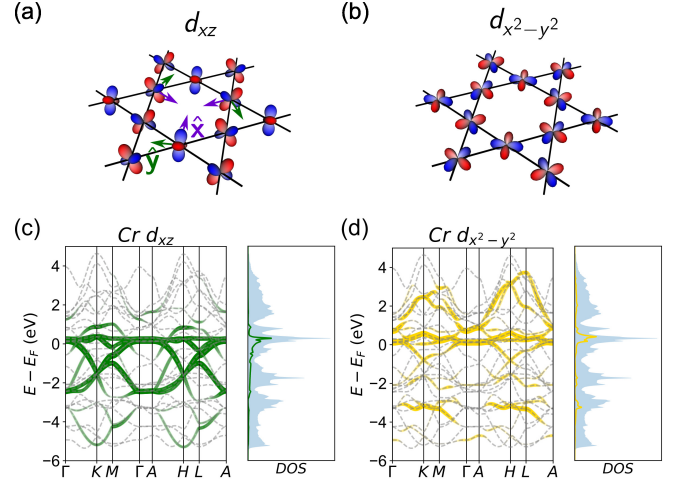


FIG. 2. (a) The shape of the d_{xz} orbitals on the chromium atoms. The basis vectors \hat{x}, \hat{y} of local coordinate frame on each Kagome site are represented by the purple and green arrows, respectively. Note that the orientation of the principle axes on different Kagome sites are chosen differently. (b) The shape of the $d_{x^2-y^2}$ orbitals on the chromium atoms. (c) Band structure and the local density of states (LDOS) projected onto the d_{xz} orbitals. (d) Band structure and the LDOS projected onto the $d_{x^2-y^2}$ orbitals. In the LDOS plots, the light blue shadows stand for the total LDOS.

bitals, and the Sb-5p orbitals. Indeed, these orbitals are all responsible for the low energy physics near the Fermi level, as suggested by *ab initio* studies [16, 30]. In Fig. 1(a) we provide the band dispersion, whose color codes stand for the weights of different orbital content, and the corresponding local density of states (LDOS) obtained from density functional theory using VASP [31, 32] and GGA [33]. The total density of states approaches its peak at around ~ 300 meV above the Fermi level, which are mostly formed by the Cr- d_{xz} and d_{yz} orbitals. The d_{z^2} and $d_{x^2-y^2}$ orbitals are also responsible for states close to E_F . Except for these Cr orbitals, we also found that the Sb_1 - p_z orbital provides a electron pocket near the Γ point, which is highlighted by the red markers in Fig. 1(a). The Sb_2 - p_{\pm} and p_z orbitals also strongly hybridize with the Cr-d orbitals, which lead to non-negligible contributions to the band structure near E_F .

We also provide the momentum resolved spectral function at the Fermi level with different k_z values obtained from the DFT band structure in Figs. 1(c) and 1(d). Three electron pockets near the M points, which are mostly formed by Cr- d_{xz} and d_{yz} orbitals, are easily visible. Furthermore, we observe near the Γ point one electron pocket formed by the Sb- p_z orbital, and hole pockets formed by Cr- d_{xz} , d_{z^2} and $d_{x^2-y^2}$ orbitals. The similarity in the Fermi pockets at $k_z = 0$ and $k_z = \pi$ planes also shows the 2-dimensional nature of this material.

This *ab initio* analysis shows that the electronic structure of CsCr_3Sb_5 is highly complex with a large amount of degrees of freedom. We conclude that a simple three-band kagome model is insufficient to describe the low-energy physics of this material. A more suitable model must be constructed with

caution.

Since there are many orbitals contributing to the low energy physics, it is a challenging task to build a reliable model which is capable of capturing the relevant physics while not being unnecessarily complicated. Hence, we first analyse the crystalline symmetry of this material. The space group of CsCr_3Sb_5 is $P6/mmm$ (no. 191). The Wyckoff positions, site-symmetry groups and irreducible representations (irrep) of these active atomic orbitals are discussed as follows [34, 35]:

- The Cr- d orbitals are at the $3f$ Wyckoff position (Kagome sites). Each of the orbitals forms a one-dimensional irrep of the site-symmetry group mmm (D_{2h}). Since all d orbitals have inversion eigenvalue $+1$, their representations are uniquely determined by the quotient group 222 (D_2). In Table I, we provide the character table and the representations of the d -orbitals of this point group. The local coordinate basis for each Kagome site is selected in accordance with the principle axes of the site symmetry group, as labeled in Fig. 2(a).
- The Sb_1 - p_z orbital is at the $1b$ Wyckoff position (triangular sites) which forms the irrep A_{2u} of the site-symmetry group $6/mmm$ (D_{6h}). The Sb_1 - p_{\pm} orbitals form the irrep E_{1u} of the site-symmetry group $6/mmm$.
- The Sb_2 - p_z and p_{\pm} orbitals are at the $4h$ Wyckoff position which form the one-dimensional irrep A_1 and two-dimensional irrep E of the site-symmetry group $3m$ (C_{3v}), respectively.
- One empty Cs band is around 2eV above the Fermi level, which also hybridizes with multiple Sb- p orbitals. The Cs- s orbital is at the $1a$ Wyckoff position which forms the irrep A_{1g} of the site-symmetry group $6/mmm$ (D_{6h}).

By projecting the *ab initio* Bloch states onto these atomic orbitals, one can construct an effective tight-binding model with $31 = 1 \times 1(\text{Cs-}s) + 3 \times 5(\text{Cr-}d) + 5 \times 3(\text{Sb-}p)$ orbitals and $34 = 1 \times 1(\text{Cs-}6s^1) + 3 \times 6(\text{Cr-}3d^5 4s^1) + 5 \times 3(\text{Sb-}5p^3)$ valence electrons per unit cell using wannier90 [36]. This tight-binding model can faithfully describe the energy bands in the interval $-6\text{eV} < E - E_F < 5\text{eV}$.

In Figs. 2(c-d), we provide the “fat bands” projected onto the d_{xz} and $d_{x^2-y^2}$ orbitals on the 31-band tight-binding model, with their corresponding LDOS plots. The spectral weights of the other three types of d orbitals are shown in the supplemental material (SM). Due to the strong hybridization between the Cr- d orbitals and the Sb- p orbitals, states that are a few electron-volts away from the Fermi level still possess non-negligible LDOS from these Cr- d orbitals. Among the five d orbitals, we found that the LDOS d_{xz} orbital has the smallest spread, while the LDOS of d_{yz} and $d_{x^2-y^2}$ orbitals have larger spreads than other orbitals. These results indicate that d_{xz} orbitals have weaker hybridization strength with other orbitals, implying that d_{xz} might have the strongest renormalization when the interaction effects are considered.

Interaction effects. To take the electron interactions into consideration, we choose a Hubbard-Kanamori-type Hamiltonian to describe correlation effects [28, 37], in which the on-site repulsive interaction terms and Ising-type ferromagnetic Hund’s coupling terms of Cr- d orbitals are considered:

$$H_I = U \sum_{j\alpha} \tilde{n}_{j\alpha\uparrow} \tilde{n}_{j\alpha\downarrow} + U' \sum_{j,\alpha\neq\beta} \tilde{n}_{j\alpha\uparrow} \tilde{n}_{j\beta\downarrow} + (U' - J_H) \sum_{j,\alpha<\beta,\sigma} \tilde{n}_{j\alpha\sigma} \tilde{n}_{j\beta\sigma}, \quad (1)$$

Here j stands for the Kagome lattice sites, α, β stands for the Cr- d orbital indices, and $\sigma = \uparrow, \downarrow$ stand for the electron spin. The operator $\tilde{n}_{j,\alpha,\sigma} = c_{j,\alpha,\sigma}^\dagger c_{j,\alpha,\sigma} - \frac{1}{2}$ represents the (relative) electron density on orbital α with spin σ at site j . The bare on-site Coulomb interaction on Cr- d orbitals is estimated to be around $U_{\text{bare}} \approx 12 \sim 15\text{eV}$. However, screening effects and the type of chemical environment of Cr reduce the effective interaction strength to values around $3 \sim 6\text{eV}$ [38, 39].

The interacting Hamiltonian in the correlated metallic phases can be studied by the $U(1)$ slave-spin approach [40–42]. In this framework, the quasiparticle weights and the on-site potential renormalization for each orbital can be solved self-consistently. The meaning of these renormalization factors is two-fold: (i) the quasiparticle weights which are smaller than unity indicate the suppression of the kinetic energies and the effective hybridization strength in the coherent Fermi liquid excitations; (ii) the on-site potential renormalizations may lead to charge transfer among different orbitals, while they guarantee the total filling factor to be unchanged when the interaction strength is varied. With both renormalization factors considered, the dispersion of coherent Fermi liquid excitations can be solved. In addition, the shape and the orbital contents of the Fermi surface may vary when the correlation effects are taken into consideration, due to orbital-selective correlation effects.

Here we solve the interacting Hamiltonian with interaction strength $0 \leq U \leq 6\text{eV}$ and Hund’s coupling $J_H/U = 0.2$ at a fixed filling factor. Our results indicate that: (i) orbital-selective correlation effects exist, and the d_{xz} orbital experiences the strongest renormalization; (ii) narrow bands will be pinned near the Fermi energy, leading to a considerable reduction in the energetic separation between the Fermi level and the peak of the LDOS from the *ab initio* value of 300meV. Below we further elaborate our discussion regarding these points.

Orbital-selective Mott correlation. The quasiparticle weights of all five d orbitals as functions of interaction strength U are provided in Fig. (3). Significantly, the quasiparticle weights are strongly renormalized when the interaction strength U is increased above 4eV. Moreover, the renormalization effects on distinct d orbitals are different from each other. In brief, the d orbitals which have weaker hybridization or smaller hoppings to other orbitals are more likely to be renormalized. Indeed, as shown in Fig. 3, the quasiparticle weight of d_{xz} drops the most rapidly with increasing interac-

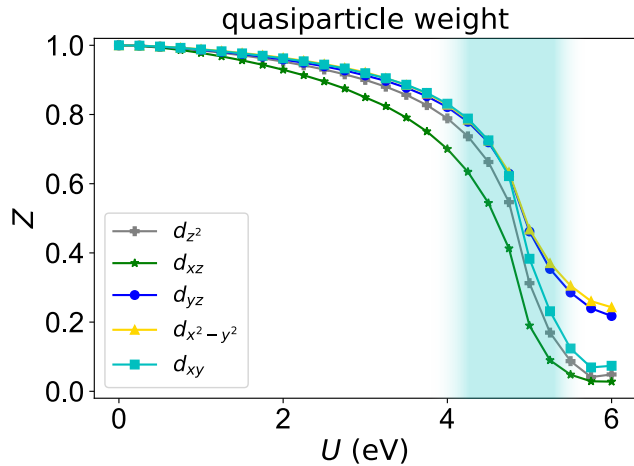


FIG. 3. quasiparticle weights and electron occupation numbers (per spin) of the five Cr- d orbitals, computed as functions of the interaction strength $0 \leq U \leq 6$ eV. The d_{xz} orbital shows the strongest renormalization effect with large interaction strength $U \gtrsim 4$ eV. In the region highlighted by the cyan shadow, the d orbitals quasiparticle weights drop significantly. The Hund's coupling strength is chosen to be $J_H = 0.2U$ in this calculation.

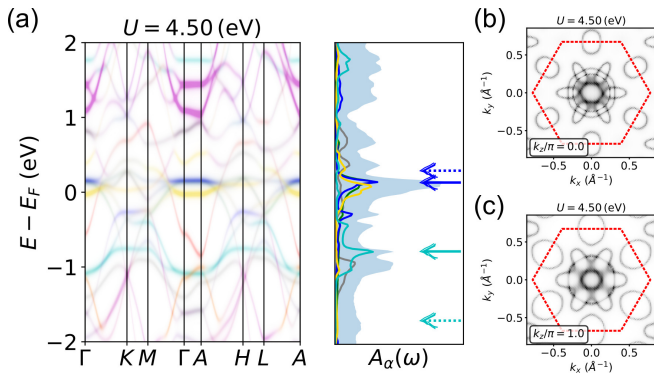


FIG. 4. (a) Momentum resolved spectral functions of coherent excitations $A_\alpha^{\text{coh}}(\mathbf{k}, \omega)$ and local density of states obtained from the slave-spin approach with interaction strength $U = 4.5$ eV. The color codes are the same as labeled in Fig. 1. Dashed arrows stand for the peaks of LDOS at $U = 0$, while solid arrows stand for the peaks of LDOS $U = 4.5$ eV. The color codes of the orbital contents are the same as in Fig. 1(a). (b-c) Fermi surface plots at the $k_z = 0$ and $k_z = \pi$ planes.

tion U . In contrast, the Z_α values of the $d_{x^2-y^2}$ and d_{yz} orbitals are also noticeably larger than for other d orbitals, especially when $U \gtrsim 5$ eV. We also note that three of the orbitals d_{xz} , d_{z^2} and d_{xy} are strongly renormalized by $Z \lesssim 0.1$ when the interaction is increased to $U = 6$ eV, which still falls within reasonably estimated ranges [38, 39]. This indicates that the system is approaching an orbital-selective Mott transition, during which the quasiparticle weights of one or more orbitals decay to zero.

Emergent flat band near Fermi level. Correlation effects of quasiparticle weights and on-site potentials lead to the sup-

pression of kinetic energy and hybridization effects in the coherent Fermi liquid spectrum. In Fig. 4(a), the orbital-resolved coherent fermion excitation spectrum $A_\alpha^{\text{coh}}(\mathbf{k}, \omega)$ and its corresponding LDOS with interaction strength $U = 4.5$ eV are provided. The band structure is drastically changed compared to the band structure without correlation effects [Fig. 1(a)]. The dashed arrows in Fig. 4(a) label the position of two LDOS peaks in the *ab initio* band structure, while the solid arrows are the corresponding peaks in the correlated LDOS. The peak above E_F labeled by the blue arrow, which is mostly formed by d_{xz} , d_{yz} and $d_{x^2-y^2}$ orbitals, now appears considerably closer to the Fermi energy. At the same time, the occupied ‘‘flat band’’ of the d_{xy} orbital, which is highlighted by the cyan arrows, is strongly pushed upward. Although the emergent ‘‘flat bands’’ of the coherent excitations appear near E_F , the reduction of the quasiparticle weights also leads to weaker intensities in the momentum resolved spectral functions.

The correlated Fermi surfaces are also shown in Figs. 4(b) and 4(c). Due to orbital-selective renormalization effects, the size and shape of Fermi pockets with different orbital contents will be changed. For example, the electron pockets around the three M points become smaller than the ones in Fig. 1(c). The concentric Fermi pockets around the Γ point, which are predominantly formed by p_z , d_{xz} and $d_{x^2-y^2}$ orbitals, have as well different sizes than their counterparts without correlation effect. Moreover, another shallow electron pocket emerges around Γ point, which is mostly formed by the $d_{x^2-y^2}$ orbital. Additional discussion regarding the correlated Fermi surfaces with different interaction strengths U can also be found in SM [42].

Discussion. Given that CsCr_3Sb_5 is new and strongly correlated with active flat bands, and considering the extensive ongoing interest in its more weakly correlated V-based counterpart [21], we can expect the Cr-based Kagome material to reveal much new insight into the strong correlation physics of metallic systems with magnetically frustrated lattices. Here we have analyzed its the symmetries and electronic states. Based on an effective 31-orbital tight-binding model that faithfully describes the *ab initio* band structure, we are able to study correlation effects on the Cr- d orbitals by the slave-spin approach. Our results unveil that the renormalization effects are significantly large when the interaction strength is within a reasonable and realistic range. Due to the inequivalence of the Cr- d orbitals as irreps of the point group D_{2h} , the correlation effects show a noticeable orbital-selective signature, with the d_{xz} orbital experiencing the strongest renormalization. The strong renormalization effect suggests that fluctuations in the spin and other collective channels will have considerable spectral weight, and this can be tested by neutron scattering or resonant inelastic X-ray spectroscopy.

Our study also provides predictions about the electronic structure of this material. We identify flat bands that lie in the immediate vicinity of the Fermi energy, in contrast to the noninteracting flat bands that appear about 0.3 eV away from the Fermi energy. Furthermore, we determine the shape and size of the Fermi pockets in the presence of interactions.

These effects can be tested by measurements such as angle resolved photoemission spectroscopy and scanning tunneling microscopy.

Our construction and analysis of the electronic states based on crystalline symmetries set the stage for further in-depth study of the competing ground states and quantum criticality in this new correlated material. The fact that d_{xz} and d_{yz} states dominate the low-energy states suggest the construction of either corresponding quasi-molecular orbitals [43, 44], which have the advantage of incorporating the low-energy p and d states in a symmetry-compatible way, or the compact molecular orbitals [14, 15], which address the role of topology. Such real state basis will allow for the treatment of competing *effective* interactions for both the development of electronic orders and the amplification of quantum fluctuations. The topological nature of the electronic bands becomes clear once the spin-orbit coupling is taken into consideration [42]. The electronic topology may also entwine charge and spin degrees of freedom in the symmetry broken ordered phases [10, 45]. In other kagome compounds, novel density wave phases that break time-reversal symmetry have been evidenced [6, 9, 46, 47]; the extent to which such unusual electronic order develops in CsCr_3Sb_5 is yet another fascinating question for the future.

Note added: During the preparation of this manuscript, Ref. [48] appeared on the arXiv preprint server studying CsCr_3Sb_5 using the DFT + DMFT approach: where there is overlap, concerning the orbital-selective correlation effect, their results are compatible with ours; however, Fermi surface under correlation and systematic symmetry analysis are not addressed in their work.

We thank Pengcheng Dai, Ming Yi, Yucheng Guo and Zehao Wang for useful discussions. Work at Rice has primarily been supported by the U.S. DOE, BES, under Award No. DE-SC0018197 (model construction, F.X., Y.F., Y.H.), by the Air Force Office of Scientific Research under Grant No. FA9550-21-1-0356 (orbital-selective correlations and model calculations, F.X., Y.F., L.C., S.S., C.S.), by the Robert A. Welch Foundation Grant No. C-1411 and the Vannevar Bush Faculty Fellowship ONR-VB N00014-23-1-2870 (Q.S.). The majority of the computational calculations have been performed on the Shared University Grid at Rice funded by NSF under Grant EIA-0216467, a partnership between Rice University, Sun Microsystems, and Sigma Solutions, Inc., the Big-Data Private-Cloud Research Cyberinfrastructure MRI-award funded by NSF under Grant No. CNS-1338099, and the Extreme Science and Engineering Discovery Environment (XSEDE) by NSF under Grant No. DMR170109. Y.L. acknowledges funding by the National Natural Science Foundation of China (Grant No. 12004296). R.V. acknowledges funding by the Deutsche Forschungsgemeinschaft (DFG, German Research Foundation) through Project No. TRR 288 — 422213477 (project A05).

- [1] A. Mielke, *Journal of Physics A: Mathematical and General* **25**, 4335 (1992).
- [2] Y.-P. Lin, C. Liu, and J. E. Moore, *arXiv e-prints*, [arXiv:2307.11810](https://arxiv.org/abs/2307.11810) (2023), [arXiv:2307.11810](https://arxiv.org/abs/2307.11810) [cond-mat.str-el].
- [3] D. Călugăru, A. Chew, L. Elcoro, Y. Xu, N. Regnault, Z.-D. Song, and B. A. Bernevig, *Nature Physics* **18**, 185 (2022).
- [4] Y.-X. Jiang, J.-X. Yin, M. M. Denner, N. Shumiya, B. R. Ortiz, J. He, X. Liu, S. S. Zhang, G. Chang, I. Belopolski, *et al.*, *Nature Materials* **20**, 1353 (2021).
- [5] M. Kang, S. Fang, L. Ye, H. C. Po, J. Denlinger, C. Jozwiak, A. Bostwick, E. Rotenberg, E. Kaxiras, J. G. Checkelsky, *et al.*, *Nature communications* **11**, 1 (2020).
- [6] C. Mielke, D. Das, J.-X. Yin, H. Liu, R. Gupta, Y.-X. Jiang, M. Medarde, X. Wu, H. C. Lei, J. Chang, P. Dai, Q. Si, H. Miao, R. Thomale, T. Neupert, Y. Shi, R. Khasanov, M. Z. Hasan, H. Luetkens, and Z. Guguchia, *Nature* **602**, 245 (2022).
- [7] S. Zhou and Z. Wang, *Nature Communications* **13**, 7288 (2022).
- [8] X. Teng, L. Chen, F. Ye, E. Rosenberg, Z. Liu, J.-X. Yin, Y.-X. Jiang, J. S. Oh, M. Z. Hasan, K. J. Neubauer, B. Gao, Y. Xie, M. Hashimoto, D. Lu, C. Jozwiak, A. Bostwick, E. Rotenberg, R. J. Birgeneau, J.-H. Chu, M. Yi, and P. Dai, *Nature* **609**, 490 (2022).
- [9] J.-X. Yin, Y.-X. Jiang, X. Teng, M. S. Hossain, S. Mardanya, T.-R. Chang, Z. Ye, G. Xu, M. M. Denner, T. Neupert, B. Lienhard, H.-B. Deng, C. Setty, Q. Si, G. Chang, Z. Guguchia, B. Gao, N. Shumiya, Q. Zhang, T. A. Cochran, D. Multer, M. Yi, P. Dai, and M. Z. Hasan, *Phys. Rev. Lett.* **129**, 166401 (2022).
- [10] C. Setty, C. A. Lane, L. Chen, H. Hu, J.-X. Zhu, and Q. Si, *arXiv e-prints*, [arXiv:2203.01930](https://arxiv.org/abs/2203.01930) (2022), [arXiv:2203.01930](https://arxiv.org/abs/2203.01930) [cond-mat.str-el].
- [11] J. Huang, L. Chen, Y. Huang, C. Setty, B. Gao, Y. Shi, Z. Liu, Y. Zhang, T. Yilmaz, E. Vescovo, M. Hashimoto, D. Lu, B. I. Yakobson, P. Dai, J.-H. Chu, Q. Si, and M. Yi, *Nature Physics* [10.1038/s41567-023-02362-3](https://doi.org/10.1038/s41567-023-02362-3) (2024).
- [12] L. Ye, S. Fang, M. Kang, J. Kaufmann, Y. Lee, C. John, P. M. Neves, S. Y. F. Zhao, J. Denlinger, C. Jozwiak, A. Bostwick, E. Rotenberg, E. Kaxiras, D. C. Bell, O. Xanson, R. Comin, and J. G. Checkelsky, *Nature Physics* [10.1038/s41567-023-02360-5](https://doi.org/10.1038/s41567-023-02360-5) (2024).
- [13] S. Adhitha Ekahana, Y. Soh, A. Tamai, D. Gosálbez-Martínez, M. Yao, A. Hunter, W. Fan, Y. Wang, J. Li, A. Kleibert, C. A. F. Vaz, J. Ma, Y. Xiong, O. V. Yazyev, F. Baumberger, M. Shi, and G. Aeppli, *arXiv e-prints*, [arXiv:2206.13750](https://arxiv.org/abs/2206.13750) (2022), [arXiv:2206.13750](https://arxiv.org/abs/2206.13750) [cond-mat.str-el].
- [14] L. Chen, F. Xie, S. Sur, H. Hu, S. Paschen, J. Cano, and Q. Si, *arXiv e-prints*, [arXiv:2307.09431](https://arxiv.org/abs/2307.09431) (2023), [arXiv:2307.09431](https://arxiv.org/abs/2307.09431) [cond-mat.str-el].
- [15] H. Hu and Q. Si, *Science Advances* **9**, eadg0028 (2023).
- [16] Y. Liu, Z.-Y. Liu, J.-K. Bao, P.-T. Yang, L.-W. Ji, J.-Y. Liu, C.-C. Xu, W.-Z. Yang, W.-L. Chai, J.-Y. Lu, C.-C. Liu, B.-S. Wang, H. Jiang, Q. Tao, Z. Ren, X.-F. Xu, C. Cao, Z.-A. Xu, J.-G. Cheng, and G.-H. Cao, *arXiv e-prints*, [arXiv:2309.13514](https://arxiv.org/abs/2309.13514) (2023), [arXiv:2309.13514](https://arxiv.org/abs/2309.13514) [cond-mat.supr-con].
- [17] J.-X. Yin, B. Lian, and M. Z. Hasan, *Nature* **612**, 647 (2022).
- [18] B. R. Ortiz, L. C. Gomes, J. R. Morey, M. Winiarski, M. Bordelon, J. S. Mangum, I. W. H. Oswald, J. A. Rodríguez-Rivera, J. R. Neilson, S. D. Wilson, E. Ertekin, T. M. McQueen, and E. S. Toberer, *Phys. Rev. Mater.* **3**, 094407 (2019).
- [19] B. R. Ortiz, S. M. L. Teicher, Y. Hu, J. L. Zuo, P. M. Sarte, E. C. Schueller, A. M. M. Abeykoon, M. J. Krogstad, S. Rosenkranz, R. Osborn, R. Seshadri, L. Balents, J. He, and S. D. Wilson,

- Phys. Rev. Lett.* **125**, 247002 (2020).
- [20] B. R. Ortiz, P. M. Sarte, E. M. Kenney, M. J. Graf, S. M. Teicher, R. Seshadri, and S. D. Wilson, *Physical Review Materials* **5**, 034801 (2021).
- [21] S. D. Wilson and B. R. Ortiz, *arXiv e-prints*, [arXiv:2311.05946](https://arxiv.org/abs/2311.05946) (2023), [arXiv:2311.05946](https://arxiv.org/abs/2311.05946) [cond-mat.supr-con].
- [22] H. Zhao, H. Li, B. R. Ortiz, S. M. Teicher, T. Park, M. Ye, Z. Wang, L. Balents, S. D. Wilson, and I. Zeljkovic, *Nature* <https://doi.org/10.1038/s41586-021-03946-w> (2021).
- [23] X. Zhou, Y. Li, X. Fan, J. Hao, Y. Dai, Z. Wang, Y. Yao, and H.-H. Wen, *arXiv e-prints*, [arXiv:2104.01015](https://arxiv.org/abs/2104.01015) (2021), [arXiv:2104.01015](https://arxiv.org/abs/2104.01015) [cond-mat.supr-con].
- [24] Z. Liang, X. Hou, F. Zhang, W. Ma, P. Wu, Z. Zhang, F. Yu, J.-J. Ying, K. Jiang, L. Shan, Z. Wang, and X.-H. Chen, *Phys. Rev. X* **11**, 031026 (2021).
- [25] E. Uykur, B. R. Ortiz, S. D. Wilson, M. Dressel, and A. A. Tsirlin, *npj Quantum Materials* **7**, 16 (2022).
- [26] H. Li, T. T. Zhang, T. Yilmaz, Y. Y. Pai, C. E. Marvinney, A. Said, Q. W. Yin, C. S. Gong, Z. J. Tu, E. Vescovo, C. S. Nelson, R. G. Moore, S. Murakami, H. C. Lei, H. N. Lee, B. J. Lawrie, and H. Miao, *Phys. Rev. X* **11**, 031050 (2021).
- [27] Y. Hu, S. M. Teicher, B. R. Ortiz, Y. Luo, S. Peng, L. Huai, J. Ma, N. Plumb, S. D. Wilson, J.-F. He, *et al.*, *arXiv preprint arXiv:2104.12725* (2021).
- [28] J. Kanamori, *Progress of Theoretical Physics* **30**, 275 (1963), <https://academic.oup.com/ptp/article-pdf/30/3/275/5278869/30-3-275.pdf>.
- [29] A. Georges, L. d. Medici, and J. Mravlje, *Annu. Rev. Condens. Matter Phys.* **4**, 137 (2013).
- [30] C. Xu, S. Wu, G.-X. Zhi, G. Cao, J. Dai, C. Cao, X. Wang, and H.-Q. Lin, *arXiv e-prints*, [arXiv:2309.14812](https://arxiv.org/abs/2309.14812) (2023), [arXiv:2309.14812](https://arxiv.org/abs/2309.14812) [cond-mat.supr-con].
- [31] G. Kresse and J. Furthmüller, *Phys. Rev. B* **54**, 11169 (1996).
- [32] G. Kresse and D. Joubert, *Phys. Rev. B* **59**, 1758 (1999).
- [33] J. P. Perdew, K. Burke, and M. Ernzerhof, *Phys. Rev. Lett.* **77**, 3865 (1996).
- [34] B. Bradlyn, L. Elcoro, J. Cano, M. G. Vergniory, Z. Wang, C. Felser, M. I. Aroyo, and B. A. Bernevig, *Nature* **547**, 298 (2017).
- [35] L. Elcoro, B. Bradlyn, Z. Wang, M. G. Vergniory, J. Cano, C. Felser, B. A. Bernevig, D. Orobengoa, G. de la Flor, and M. I. Aroyo, *Journal of Applied Crystallography* **50**, 1457 (2017).
- [36] G. Pizzi, V. Vitale, R. Arita, S. Blügel, F. Freimuth, G. Géranton, M. Gibertini, D. Gresch, C. Johnson, T. Koretsune, J. Ibañez-Azpiroz, H. Lee, J.-M. Lihm, D. Marchand, A. Marrazzo, Y. Mokrousov, J. I. Mustafa, Y. Nohara, Y. Nomura, L. Paulatto, S. Poncé, T. Ponweiser, J. Qiao, F. Thöle, S. S. Tsirkin, M. Wierzbowska, N. Marzari, D. Vanderbilt, I. Souza, A. A. Mostofi, and J. R. Yates, *Journal of Physics: Condensed Matter* **32**, 165902 (2020).
- [37] A. Georges, L. d. Medici, and J. Mravlje, *Annual Review of Condensed Matter Physics* **4**, 137 (2013), <https://doi.org/10.1146/annurev-conmatphys-020911-125045>.
- [38] D. Soriano, A. N. Rudenko, M. I. Katsnelson, and M. Rösner, *npj Computational Materials* **7**, 162 (2021).
- [39] L. Vaugier, H. Jiang, and S. Biermann, *Phys. Rev. B* **86**, 165105 (2012).
- [40] R. Yu and Q. Si, *Phys. Rev. B* **86**, 085104 (2012).
- [41] R. Yu and Q. Si, *Phys. Rev. B* **84**, 235115 (2011).
- [42] See the supplemental material.
- [43] I. I. Mazin, H. O. Jeschke, K. Foyevtsova, R. Valentí, and D. I. Khomskii, *Phys. Rev. Lett.* **109**, 197201 (2012).
- [44] K. Foyevtsova, H. O. Jeschke, I. Mazin, D. Khomskii, and R. Valentí, *Physical Review B* **88**, 035107 (2013).
- [45] C. Setty, H. Hu, L. Chen, and Q. Si, Electron correlations and t -breaking density wave order in a \mathbb{Z}_2 kagome metal (2021), [arXiv:2105.15204](https://arxiv.org/abs/2105.15204) [cond-mat.str-el].
- [46] L. Yu, C. Wang, Y. Zhang, M. Sander, S. Ni, Z. Lu, S. Ma, Z. Wang, Z. Zhao, H. Chen, K. Jiang, Y. Zhang, H. Yang, F. Zhou, X. Dong, S. L. Johnson, M. J. Graf, J. Hu, H.-J. Gao, and Z. Zhao, *arXiv e-prints*, [arXiv:2107.10714](https://arxiv.org/abs/2107.10714) (2021), [arXiv:2107.10714](https://arxiv.org/abs/2107.10714) [cond-mat.supr-con].
- [47] Q. Wu, Z. X. Wang, Q. M. Liu, R. S. Li, S. X. Xu, Q. W. Yin, C. S. Gong, Z. J. Tu, H. C. Lei, T. Dong, and N. L. Wang, The large static and pump-probe kerr effect with two-fold rotation symmetry in kagome metal csv_3sb_5 (2021), [arXiv:2110.11306](https://arxiv.org/abs/2110.11306) [cond-mat.supr-con].
- [48] Y. Wang, *arXiv e-prints*, [arXiv:2401.16770](https://arxiv.org/abs/2401.16770) (2024), [arXiv:2401.16770](https://arxiv.org/abs/2401.16770) [cond-mat.str-el].

SUPPLEMENTAL MATERIAL

SLAVE-SPIN APPROACH

In this section, the $U(1)$ slave-spin approach [40] is briefly reviewed. We first assume that the kinetic Hamiltonian has the following tight-binding form:

$$H_0 = \sum_{\mathbf{k}\alpha\beta\sigma} t_{\alpha\beta}(\mathbf{k}) c_{\mathbf{k}\alpha\sigma}^\dagger c_{\mathbf{k}\beta\sigma} + \sum_{\mathbf{k}\alpha\sigma} \tilde{\epsilon}_\alpha c_{\mathbf{k}\alpha\sigma}^\dagger c_{\mathbf{k}\alpha\sigma}, \quad (\text{S1})$$

in which the kinetic matrix $t_{\alpha\beta}(\mathbf{k})$ only contains the elements corresponding to the *hoppings* and *hybridizations*. All terms that correspond to the on-site potentials are denoted as $\tilde{\epsilon}_\alpha$, and are not included in $t_{\alpha\beta}(\mathbf{k})$. In this kinetic Hamiltonian H_0 , the orbital indices α, β run through all of the Cr-*d*, Sb-*p* and Cs orbitals in the 31-band model. The interaction Hamiltonian will be chosen as the form shown in Eq. (1) in the main text, in which the repulsive U and the Hund's coupling J_H only apply on the Cr-*d* orbitals.

Each local fermionic operator $c_{j\alpha\sigma}^\dagger$ is mapped to a product of two parton operators:

$$c_{j\alpha\sigma}^\dagger \rightarrow f_{j\alpha\sigma}^\dagger o_{j\alpha\sigma}^\dagger, \quad (\text{S2})$$

Here, $f_{j\alpha\sigma}^\dagger$ is fermionic, and $o_{j\alpha\sigma}^\dagger$ is a spin- $\frac{1}{2}$ operator, which acts on a local 2-dimensional Hilbert space. In the framework of $U(1)$ slave-spin theory, the spin operator o^\dagger has the following form:

$$o_{j\alpha\sigma}^\dagger = P_{j\alpha\sigma}^+ S_{j\alpha\sigma}^+ P_{j\alpha\sigma}^-, \quad P_{j\alpha\sigma}^\pm = \frac{1}{\sqrt{\frac{1}{2} \pm S_{j\alpha\sigma}^z}}, \quad (\text{S3})$$

Because of this parton construction, the local Hilbert space dimension is increased from 2 to 4. A local constraint of the physical Hilbert space is required. We introduce Lagrange multiplier terms for each orbital into the parton Hamiltonian:

$$H_\lambda = \sum_{j\alpha\sigma} \lambda_\alpha \left(S_{j\alpha\sigma}^z + \frac{1}{2} - f_{j\alpha\sigma}^\dagger f_{j\alpha\sigma} \right), \quad (\text{S4})$$

and the local constraint $\langle S_{j\alpha\sigma}^z \rangle + 1/2 = \langle f_{j\alpha\sigma}^\dagger f_{j\alpha\sigma} \rangle$ can be satisfied on the mean field level by controlling the values of λ_α . The kinetic Hamiltonian can be written as the following form using these operators:

$$H_0 = \sum_{ij\alpha\beta\sigma} t_{\alpha\beta}^{ij} f_{i\alpha\sigma}^\dagger f_{j\beta\sigma} o_{i\alpha\sigma}^\dagger o_{j\beta\sigma} + \sum_{j\alpha\sigma} (\epsilon_\alpha - \lambda_\alpha) f_{j\alpha\sigma}^\dagger f_{j\alpha\sigma}, \quad (\text{S5})$$

in which $t_{\alpha\beta}^{ij}$ is the Fourier transformation of $t_{\alpha\beta}(\mathbf{k})$ represented in real space indices. The hopping terms can then be decomposed using a ‘‘mean-field’’ assumption and a ‘‘single-site approximation’’ for the slave-spin operators:

$$f_{i\alpha\sigma}^\dagger f_{j\beta\sigma} o_{i\alpha\sigma}^\dagger o_{j\beta\sigma} \rightarrow \langle o_{i\alpha\sigma}^\dagger \rangle \langle o_{j\beta\sigma} \rangle f_{i\alpha\sigma}^\dagger f_{j\beta\sigma} + \langle f_{i\alpha\sigma}^\dagger f_{j\beta\sigma} \rangle \left(\langle o_{i\alpha\sigma}^\dagger \rangle o_{j\beta\sigma} + o_{i\alpha\sigma}^\dagger \langle o_{j\beta\sigma} \rangle \right). \quad (\text{S6})$$

We will then assume the ‘‘condensate’’ of the slave-spin operators correspond to a translation invariant non-magnetic state, such that $\langle o_{i\alpha\sigma}^\dagger \rangle = \langle o_{i\alpha\bar{\sigma}}^\dagger \rangle = \langle o_{j\alpha\sigma}^\dagger \rangle = \sqrt{Z_\alpha}$. A Taylor expansion can also be applied to the o^\dagger operators, which can lead to a simpler form:

$$o_{j\alpha\sigma}^\dagger \approx \frac{S_{j\alpha\sigma}^+}{\sqrt{n_\alpha(1-n_\alpha)}} + \sqrt{Z_\alpha} \eta_\alpha \left[2S_{j\alpha\sigma}^z - (2n_\alpha - 1) \right], \quad (\text{S7})$$

in which $\eta_\alpha = \frac{1}{2} \frac{n_\alpha - 1/2}{n_\alpha(1-n_\alpha)}$ and $n_\alpha = \langle f_{j\alpha\sigma}^\dagger f_{j\alpha\sigma} \rangle$ is the fermion density. Here the site and spin indices j, σ are omitted in the notation n_α , because we assume that the solution is translation invariant and non-magnetic.

Applying Eq. (S6) to Eq. (S5), the kinetic Hamiltonian can be separated into two parts, one of which only contains the slave-spin operators. Moreover, slave-spin operators on different lattice sites are decoupled from each other because of the single-site approximation in Eq. (S7). Combining these terms with the local interaction terms, the Hamiltonian of the slave-spin operators

can be written as follows:

$$H^S = U \sum_{\alpha} S_{\alpha\uparrow}^z S_{\alpha\downarrow}^z + U' \sum_{\alpha \neq \beta} S_{\alpha\uparrow}^z S_{\beta\downarrow}^z + (U' - J_H) \sum_{\alpha < \beta, \sigma} S_{\alpha\sigma}^z S_{\beta\sigma}^z + \sum_{\alpha\sigma} \lambda_{\alpha} S_{\alpha\sigma}^z + \sum_{\alpha\sigma} \left[h_{\alpha} \frac{S_{\alpha\sigma}^+}{\sqrt{n_{\alpha}(1-n_{\alpha})}} + \text{H.c.} \right], \quad (\text{S8})$$

in which the ‘‘bath’’ fields h_{α} are given by:

$$h_{\alpha} = \frac{1}{N} \sum_{\mathbf{k}\beta} t_{\alpha\beta}(\mathbf{k}) \sqrt{Z_{\beta}} \langle f_{\mathbf{k}\alpha\sigma}^{\dagger} f_{\mathbf{k}\beta\sigma} \rangle. \quad (\text{S9})$$

Note that H^S contains parameters that are determined by the expectation values of slave-fermion operators, such as $n_{\alpha} = \langle f_{j\alpha\sigma}^{\dagger} f_{j\alpha\sigma} \rangle$. The other part of the mean-field decomposition of H_0 , which only contains the quadratic terms of slave-fermion operators, will have parameters that are determined by the expectation of the slave-spin operators, such as $\sqrt{Z_{\alpha}} = \langle o_{j\alpha\sigma}^{\dagger} \rangle$. The slave-fermion Hamiltonian reads:

$$H^f = \sum_{\mathbf{k}\alpha\beta\sigma} h_{\alpha\beta}^f(\mathbf{k}) f_{\mathbf{k}\alpha\sigma}^{\dagger} f_{\mathbf{k}\beta\sigma}, \quad (\text{S10})$$

$$h_{\alpha\beta}^f(\mathbf{k}) = \sqrt{Z_{\alpha} Z_{\beta}} t_{\alpha\beta}(\mathbf{k}) + \delta_{\alpha\beta} (\tilde{\epsilon}_{\alpha} - \lambda_{\alpha} + \lambda_{\alpha}^0 - E_F). \quad (\text{S11})$$

in which E_F is the Fermi level determined via the filling factor. The parameters λ_{α}^0 are defined as:

$$\lambda_{\alpha}^0 = \sqrt{Z_{\alpha}} h_{\alpha} \frac{2n_{\alpha} - 1}{n_{\alpha}(1 - n_{\alpha})}, \quad (\text{S12})$$

which originate from the second term on the right-hand-side of Eq. (S7). For a given total filling factor, these mean-field parameters $\sqrt{Z_{\alpha}}$, n_{α} , λ_{α} , λ_{α}^0 and E_F can all be solved self-consistently.

Eigenvalues of the slave-fermion Hamiltonian $h^f(\mathbf{k})$ provide the dispersion of the coherent excitations, in which $Z_{\alpha} = \langle o_{j\alpha\sigma}^{\dagger} \rangle \langle o_{j\alpha\sigma} \rangle$ stand for the quasiparticle weight, and $\Delta\tilde{\epsilon}_{\alpha} = \lambda_{\alpha}^0 - \lambda_{\alpha}$ stand for the on-site energy renormalization of orbital α . Note that only the Cr- d orbitals have non-trivial Z_{α} , λ_{α} and λ_{α}^0 values. For the Sb- p orbitals, we always have $Z_{\alpha} = 1$ and $\lambda_{\alpha} = \lambda_{\alpha}^0$. Consequently, the coherent part of the Green’s function will have the following form:

$$G_{\alpha\beta}^{\text{coh}}(\mathbf{k}, z) = \sqrt{Z_{\alpha} Z_{\beta}} [\omega - h^f(\mathbf{k})]_{\alpha\beta}^{-1}, \quad (\text{S13})$$

and the corresponding momentum-resolved spectral function of orbital α can be written as:

$$A_{\alpha}^{\text{coh}}(\mathbf{k}, \omega) = -\frac{1}{\pi} \text{Im} G_{\alpha\alpha}^{\text{coh}}(\mathbf{k}, \omega + i0^+). \quad (\text{S14})$$

The dispersive spectral functions in Fig. 4(a) in the main text are computed using this equation. Similarly, the Fermi surface plots in Figs. 4(b-c) are also obtained from $A_{\alpha}^{\text{coh}}(\mathbf{k}, \omega = 0)$.

The spectral function defined in Eq. (S14) only contains the contributions from the coherent parts, which correspond to the ground state of the slave-spin Hamiltonian H^S . To compute the LDOS of the Cr- d orbitals, one needs to take the excited states of H^S into consideration [41]:

$$A_{\alpha}^{\text{loc}}(\omega) = \frac{1}{N} \sum_{\mathbf{k}} \sum_m \left(\sum_{i, \epsilon_{\mathbf{k},i} > 0} \delta(\omega + E_g - E_m - \epsilon_{\mathbf{k},i}) |u_{\alpha,i}(\mathbf{k})|^2 \frac{|\langle m | S_{\alpha}^+ | g \rangle|^2}{n_{\alpha}(1 - n_{\alpha})} \mathcal{F}_{\alpha,m}^+ \right. \\ \left. + \sum_{i, \epsilon_{\mathbf{k},i} < 0} \delta(\omega - E_g + E_m - \epsilon_{\mathbf{k},i}) |u_{\alpha,i}(\mathbf{k})|^2 \frac{|\langle m | S_{\alpha}^- | g \rangle|^2}{n_{\alpha}(1 - n_{\alpha})} \mathcal{F}_{\alpha,m}^- \right), \quad (\text{S15})$$

in which E_m and $|m\rangle$ stand for the eigenvalues and eigenstates of H^S . Specifically, $m = g$ represents the ground state. The dispersion relation $\epsilon_{\mathbf{k},i}$ and the ‘‘Bloch state’’ $u_{\alpha,i}(\mathbf{k})$ are defined as the eigenvalues and eigenvectors of $h^f(\mathbf{k})$. The factors $\mathcal{F}_{\alpha,m}^{\pm}$

are given by the following expressions:

$$\mathcal{F}_{\alpha,m}^+ = \begin{cases} 1, & m = g, \\ \frac{1-Z_\alpha}{n_\alpha^{-1}-Z_\alpha}, & m \neq g, \end{cases} \quad (\text{S16})$$

$$\mathcal{F}_{\alpha,m}^- = \begin{cases} 1, & m = g, \\ \frac{1-Z_\alpha}{(1-n_\alpha)^{-1}-Z_\alpha}, & m \neq g. \end{cases} \quad (\text{S17})$$

These factors $\mathcal{F}_{\alpha,m}^\pm$ guarantee the satisfaction of the spectral function sum rules. For other orbitals, the LDOS has the same expression as in non-interacting fermion systems, with the dispersion $\epsilon_{\mathbf{k},i}$ and Bloch states $u_{\alpha,i}(\mathbf{k})$ replaced by the eigenvalues and eigenvectors of the slave-spin Hamiltonian $h^f(\mathbf{k})$:

$$A_\alpha^{\text{loc}}(\omega) = \frac{1}{N} \sum_{\mathbf{k}} \sum_i \delta(\omega - \epsilon_{v\mathbf{k},i}) |u_{\alpha,i}(\mathbf{k})|^2. \quad (\text{S18})$$

The LDOS plots in Fig. 4(a) in the main text are computed using Eqs. (S15) and (S18).

ADDITIONAL NUMERICAL RESULTS

Band structure and d_{z^2} , d_{yz} and d_{xy} orbitals

In the main text, we provided the weights of d_{xz} and $d_{x^2-y^2}$ orbitals in Fig. 2. Here in Fig. S1, we show the weights and the corresponding LDOS of the other three types of d orbitals in the band structure. Similar to the $d_{x^2-y^2}$ orbital, we note that the d_{yz} orbital also has a broader energy spread than other orbitals.

We note that the LDOS of different d orbitals are distributed in different energy ‘‘band widths’’, which effectively capture the strength of hybridization and hopping of the corresponding orbital. To quantify their effective ‘‘band widths’’, the following two quantities can be defined for each Cr- d orbital:

$$\mu_\alpha = \int_{-\infty}^{\infty} d\omega \omega A_\alpha(\omega), \quad (\text{S19})$$

$$\sigma_\alpha^2 = \int_{-\infty}^{\infty} d\omega (\omega - \mu_\alpha)^2 A_\alpha(\omega), \quad (\text{S20})$$

in which $A_\alpha(\omega)$ stands for the local density of states (spectral function) of the orbital α . μ_α and σ_α describe the ‘‘average energy’’ and ‘‘band width’’ of the corresponding orbital. In Table S1, the values of these two quantities for the Cr- d orbitals are presented. We found that the d_{xz} has the smallest value of σ_α , while the d_{yz} and $d_{x^2-y^2}$ have larger σ_α values.

Electronic structure with different interaction strength

As we have discussed in the main text, the quasiparticle weights of the Cr- d orbitals are suppressed by the interaction effects. In the mean time, the on-site potential energies and the relative filling factors of these Cr- d orbitals are also affected. In Fig. S2(a), we show the U -dependency of the on-site energy renormalization $\Delta\tilde{\epsilon}_\alpha = \lambda_\alpha^0 - \lambda_\alpha$. Qualitatively speaking, the on-site potentials of the d_{yz} and $d_{x^2-y^2}$ orbitals are pushed downward, while the other three Cr- d orbitals are pushed upward. This is compatible with the filling factors change as shown in Fig. S2(b), in which all the five Cr- d orbitals filling factors are renormalized to half-filling in the strong interaction limit. When the local interaction U is turned off, the d_{yz} and $d_{x^2-y^2}$ orbitals are below half filling, and a negative on-site energy renormalization is able to increase the filling factors of the corresponding orbitals.

We also provide the electronic structure, including the coherent spectral functions, the LDOS, and the Fermi surface structures in Figs. S3 and S4. The spectral functions shown in Fig. S3(a) are computed with interaction strength $U = 4\text{eV}$. With this interaction strength, the quasiparticle weights are renormalized to around $Z \gtrsim 0.7$, and the coherent excitation dispersion is already modified. The solid arrows, which indicate the peaks of the LDOS, are dragged closer to the Fermi level. Similar to the case discussed in the main text, the size and shape of the concentric Fermi pockets around Γ point are also changed from the ones at $U = 0$. In the case with $U = 4.25\text{eV}$ shown in Figs. S3(d-f), similar but slightly stronger correlation effects can be observed.

When the interaction is further increased to $U = 4.75\text{eV}$, the renormalization effects shown in Fig. S4(a) are even stronger. The quasiparticle weights are reduced to $Z \sim 0.2$, and stronger modification to the band structure can be seen. Besides, as shown

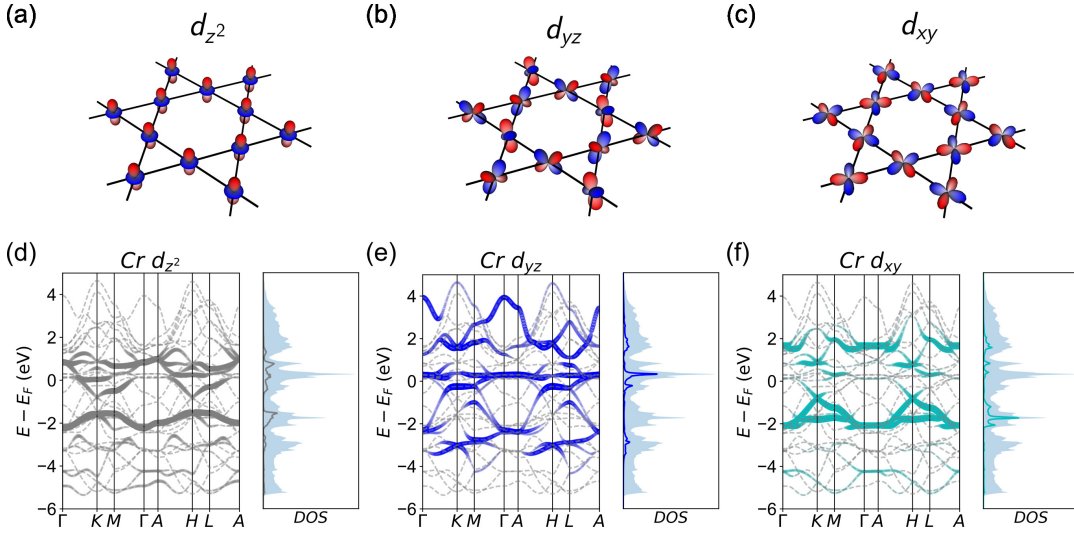


FIG. S1. (a-c) The shape and orientation of the d_{z^2} , d_{yz} and d_{xy} orbitals from the chromium atoms. (d-f) Band structures and LDOS projected onto these d orbitals. Similar to Fig. 2, the light blue shadows stand for the total LDOS.

orbital	μ_α (eV)	σ_α (eV)
d_{z^2}	-0.935	1.735
d_{xz}	-0.779	1.474
d_{yz}	-0.091	1.903
$d_{x^2-y^2}$	-0.190	1.976
d_{xy}	-0.816	1.809

TABLE S1. The local density of states distribution of the d orbitals.

in Fig. S4(b), the increased intensity near K and K' points, indicating the development of new Fermi pockets, which is another signal of modified electronic structure.

In Fig. S4(d), we show the coherent spectral functions with interaction strength $U = 5$ eV. Clearly, the LDOS peak labeled by the solid blue arrow has already been pinned extremely close to E_F , showing the possibility of an emergent flat band. The other LDOS peak, which is mostly formed by d_{xy} orbital and was around 2 eV below E_F in the *ab initio* band structure, is also pushed within $\lesssim 0.5$ eV from E_F . In addition, the Fermi surfaces, which are shown in Fig. S4(e-f), are significantly changed with interaction strength $U = 5$ eV. Except for the size and shape changes of the pockets around Γ and M , there are indeed new electron pockets around K and K' points developed. As such, this material can potentially be tuned through a Lifshitz transition.

Band structure with spin-orbit coupling

In Fig. S5, we provide the plots of the *ab initio* band structure with and without the spin-orbit coupling. As seen in Fig. S5(e), SOC could lead to some gap opening up to ~ 0.1 eV at Γ and K points.

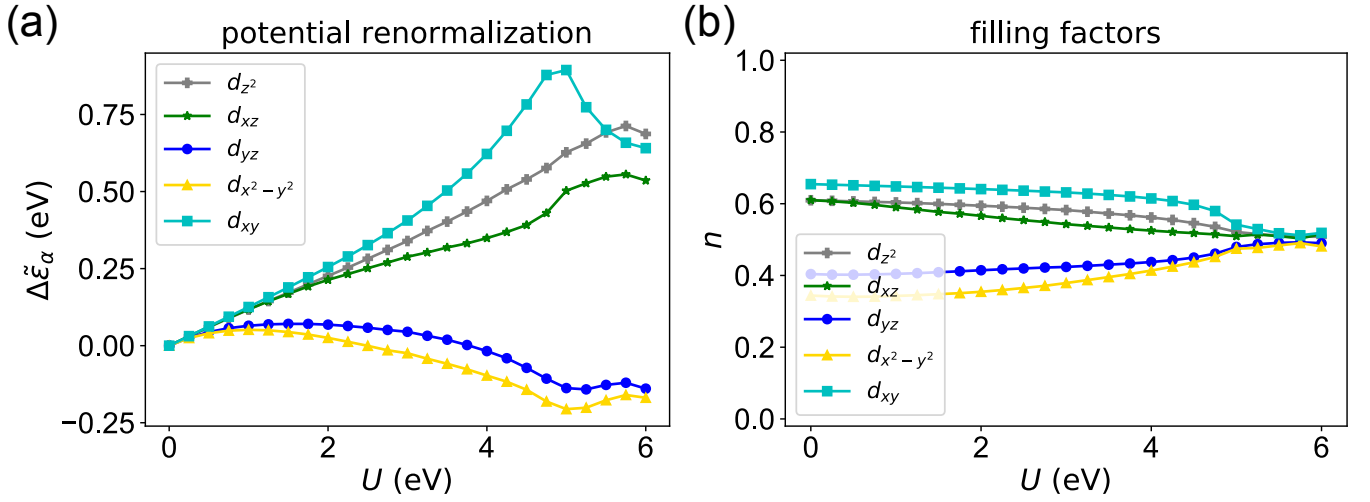


FIG. S2. (a) The on-site potential renormalization $\Delta\tilde{\epsilon}_\alpha = \lambda_\alpha^0 - \lambda_\alpha$ of each Cr- d orbital as functions of U . (b) Average particle numbers of each Cr- d orbital as functions of interaction strength U .

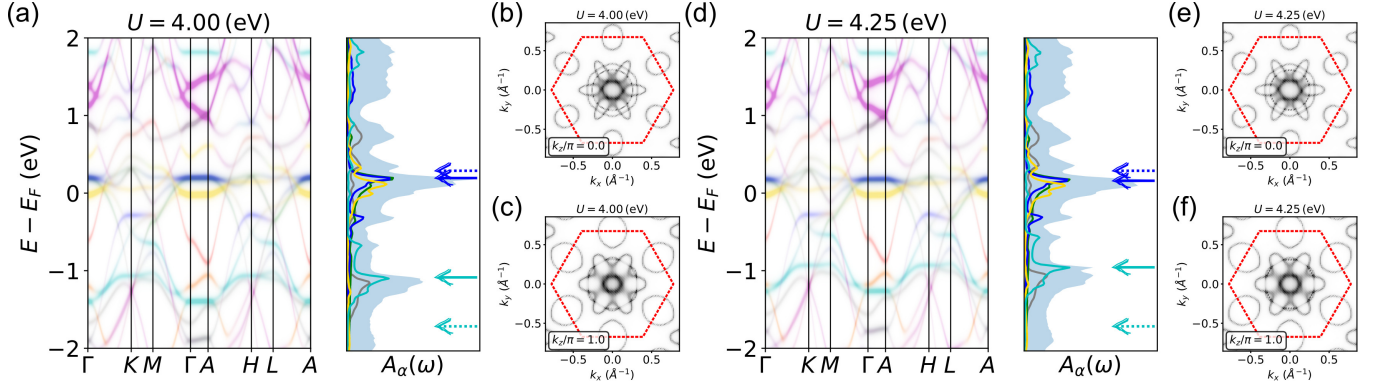


FIG. S3. (a-c) Coherent excitation dispersions, orbital-resolved LDOS and Fermi surfaces at $k_z = 0$ and $k_z = \pi$ with interaction strength $U = 4.0$ eV. (d-f) coherent dispersions, LDOS and Fermi surfaces solved with interaction strengths $U = 4.25$ eV.

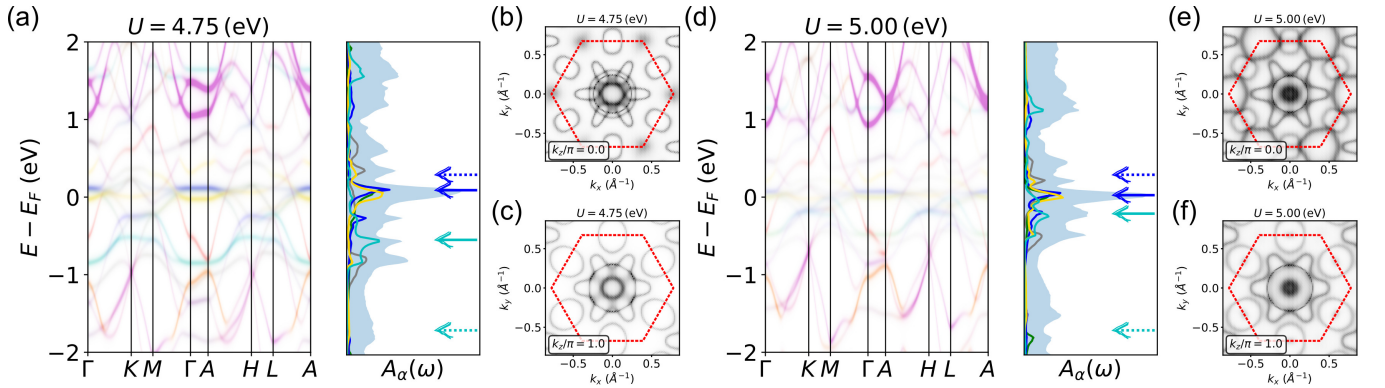


FIG. S4. (a-c) The coherent excitation dispersions, the orbital-resolved LDOS and the Fermi surfaces structures at $k_z = 0$ and $k_z = \pi$ with interaction strength $U = 4.75$ eV. (d-f) The coherent dispersions, the LDOS and the Fermi surfaces solved with interaction strengths $U = 5$ eV.

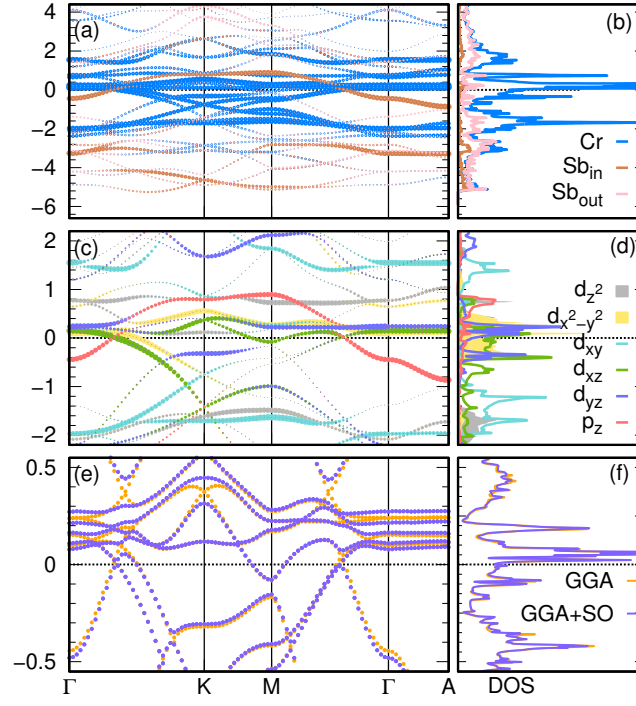


FIG. S5. (a-b) The overall band structure of CsCr₃Sb₅. (c-d) The Cr-*d* and Sb-*p* orbitals projected onto the band structure in the energy interval $-2 \text{ eV} \leq E - E_F \leq 2 \text{ eV}$. (e-f) The band structure with and without spin-orbit coupling in the energy interval $-0.5 \text{ eV} \leq E - E_F \leq 0.5 \text{ eV}$.